JCTC Journal of Chemical Theory and Computation

pubs.acs.org/JCTC Article

Synthesis of Hidden Subgroup Quantum Algorithms and Quantum Chemical Dynamics

Srinivasan S. Iyengar,* Anup Kumar, Debadrita Saha, and Amr Sabry*

Cite This: J. Chem. Theory Comput. 2023, 19, 6082−6092 Read Online

ACCESS | Metrics & More | Article Recommendations

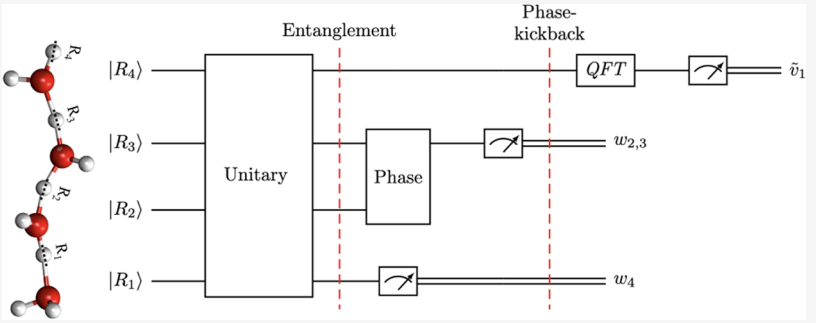

ABSTRACT: We describe a general formalism for quantum dynamics and show how this formalism subsumes several quantum algorithms, including the Deutsch, Deutsch−Jozsa, Bernstein−Vazirani, Simon, and Shor algorithms as well as the conventional approach to quantum dynamics based on tensor networks. The common framework exposes similarities among quantum algorithms and natural quantum phenomena: we illustrate this connection by showing how the correlated behavior of protons in water wire systems that are common in many biological and materials systems parallels the structure of Shor's algorithm.

1. INTRODUCTION

The promise of solving complex problems efficiently using quantum computing hardware and associated software is a rapidly evolving research frontier.[1−4] While we are in the very early stages of this upcoming quantum revolution, there are a diverse set of important scientific and technological areas that may greatly benefit from such developments. One key quantum algorithm that started this entire debate approximately 25 years ago is Shor's algorithm.[5,6] Here, a quantum system can, in principle, factorize large integers into prime factors using $O((\log N)^2(\log\log N)(\log\log\log N))$ fast multiplications.[5] Since this is exponentially faster than the traditional classical approach, which requires $O(e^{1.9(\log N)^{1/3}(\log\log N)^{2/3}})$ operations, the promise of a second quantum revolution was born.

Orthogonally, the sister fields of atomic and molecular physics and quantum chemistry have learned to wonder if atoms and molecules store and propagate quantum information. While it has been known that such "information" indeed evolves in time as per the laws of quantum theory, one may also ask if chemical reactions and chemical transformations are indeed algebraic transformations that "compute" new information not dissimilar from quantum algorithms. That is, is the time evolution of a molecular process to be interpreted as a computational protocol that is "programmed" by nature or through clever use of synthetic techniques? However, the study of molecular dynamics is complicated by the fact that molecules contain many correlated degrees of freedom. For example, with $\mathcal{D}$ degrees of freedom and $\mathcal{N}$ basis representation per degree of freedom, the complexity of information grows approximately as $\mathcal{N}^{\mathcal{D}}$. As a result, quantum chemical dynamics is thought to be exponentially hard.

To alleviate this rather catastrophic situation, tensor networks (TNs)[7,8] have recently become popular. Tensor networks have roots in the tensor decomposition field of multilinear algebra,[9,10] are a general framework for data compression,[11−14] and have proven to be effective for efficient representation of many-body quantum states in strongly correlated systems.[7,15−25] While a tensor network treatment adaptively truncates the Hilbert space based on the intrinsic entanglement within the problem, given the advent of novel quantum computing algorithms, tensor networks have also proved to be a natural resource for developing new quantum algorithms.[26−29] The approach has been shown to have applications for low-energy states of local, gapped Hamiltonians, which are characterized by satisfying a so-called area law of entanglement.[7,30,31] The introduction of the

Received: April 11, 2023
Published: September 13, 2023

https://doi.org/10.1021/acs.jctc.3c00404
J. Chem. Theory Comput. 2023, 19, 6082−6092

density matrix renormalization group (DMRG)[32−35] was perhaps the catalyst for the excitement in the TN methodology, proving to be very useful for the simulation of one-dimensional quantum lattices,[36−39] electronic structure calculations,[40−48] approximations to vibrational states,[49−56] open-quantum systems[25,57,58] and image processing,[11−14,59] and even machine learning applications.[60−62]

In this paper, we cast the basic structure present in a family of quantum algorithms that includes Shor's algorithm in an abstract fashion using the language of tensor networks.[7] This presentation exposes parallels to more general quantum processes that occur in multidimensional quantum dynamics[63−71] and in quantum dynamics of open systems[57,72−82] that are of significance to many chemical, biological, and materials problems. Hence, we will then show how such an abstraction applies directly to many natural and synthetic chemical processes, thus drawing a connection between existing quantum algorithms and chemical and natural processes.[83−87] At the end of this exposition, we are forced to ask if natural processes exist that may represent mathematically constructed, number-theoretic algorithms.

Given this overarching theme, this paper is organized as follows. In Section 2, we review the textbook presentation of Shor's algorithm and generalize it in Section 3, using tensor networks to arbitrary multipartite systems. The formalism used in that generalization leads to our central result in Section 4, which derives the correspondence to generalized Shor-like circuits applicable to general quantum chemical dynamics problems. In Section 5, we exploit it to show that multidimensional quantum dynamics in protonated water clusters such as wire systems that are present in many biological ion channels and enzyme active sites and are also the subject of several state-of-the-art experimental[88−91] and multidimensional correlated quantum dynamics studies[92−94] can be mapped to the circuit model exhibiting the same structure as the family of quantum algorithms under study. Section 6 concludes.

2. QUANTUM ALGORITHMS

Most quantum algorithms that are thought to be exponentially faster than their best-known classical counterparts are algorithms for solving instances of hidden subgroup problems. This family of algorithms includes the textbook quantum algorithms of Deutsch, Deutsch−Jozsa, Bernstein−Vazirani, Simon, and Shor[95−102] and are all solved using the same approach illustrated in Figure 1. All of the algorithms start by creating an equal superposition of all relevant possibilities, applying the U_f block to the superposition, and analyzing the result using the quantum Fourier transform (QFT). The U_f block, often called the "oracle," is uniformly defined as

$$U_f(|x\rangle|y\rangle) = |x\rangle|f(x) \oplus y\rangle \tag{1}$$

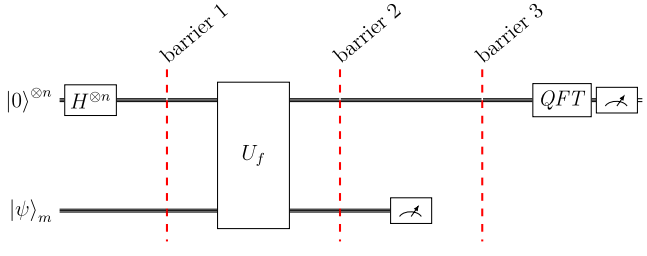

Figure 1. Template circuit for hidden subgroup problems.

for the specific function f of interest. The circuit template uses the QFT uniformly as the last step, although—with the notable exception of Shor's algorithm—the low precision approximation of QFT (which is the Hadamard gate[103]) is often sufficient.

2.1. Shor's Algorithm. To be concrete, Figure 2 instantiates the general template to the quantum circuit for an instance of Shor's algorithm for factoring the number N. In Stage (1), two registers are prepared: the top (input) register of q qubits is initialized to an equal superposition $\frac{1}{\sqrt{2^q}}\sum_{i=0}^{2^q-1}|i\rangle$. In the bottom (output) register of m qubits, each qubit is initialized to $|0\rangle$. In Stage (2), the initial state,

$$\left\{\frac{1}{\sqrt{2^q}}\sum_{i=0}^{2^q-1}|i\rangle\right\}\otimes|0\rangle \tag{2}$$

is evolved through a reversible circuit that computes $[a^x \pmod N]$. The resulting state is

$$\frac{1}{\sqrt{2^q}}\sum_{i=0}^{2^q-1}|i\rangle\otimes|a^i(\mathrm{mod}\ N)\rangle \tag{3}$$

Equation 3 represents a highly entangled state. The degree to which the two sets of registers above is entangled is probed by computing the Schmidt number from a tensor network decomposition of the unitary evolution operations that lead to eq 3, as detailed in ref 104

At Stage (3), a measurement of the output register produces some value w; this measurement collapses the input register to a superposition of these states $|i\rangle$ where $a^i \pmod N = w$. Let the number of those states be W; the input register state is then $\frac{1}{\sqrt{W}}\sum_{i=0}^{W-1}|i\rangle$ for those states $|i\rangle$ whose mapping by the function $a^x \pmod N$ produces the same value w. Since the function $a^x \pmod N$ is periodic, all of these states are guaranteed to be of the form $|a + ks\rangle$ for some starting offset a and some multiple k of the period s. Put differently, the state of the input register is

$$\sqrt{\frac{s}{W}}\sum_{k=0}^{(W/s)-1}|a + ks\rangle \tag{4}$$

It is important to note that a different measurement w' of the output register would only change the starting offset a and the total number of states W in the superposition, but it would not change the period s. Critically, the QFT is largely insensitive to the starting offset and the total number of states in the superposition. Its main effect is to transform a superposition of periodic states $|a + ks\rangle$ to states in the Fourier basis $|\tilde{v}\rangle$ such that v is close to a multiple of W/s. When the period s is a power of 2, the Fourier states are perfectly aligned with the multiple of W/s, as shown by the formula below:

$$\mathrm{QFT}\left(\sqrt{\frac{s}{W}}\sum_{k=0}^{(W/s)-1}|a + ks\rangle\right) = \frac{1}{\sqrt{s}}\sum_{m=0}^{s-1}e^{i(2\pi/s)ma}|m\tilde{W}/s\rangle \tag{5}$$

When the period is not a power of 2, the Fourier states with the largest probabilities are the ones close to a multiple of W/s. From such a measurement, some classical postprocessing succeeds, with high probability, in determining the period s and hence the factors of the number N.

2.2. Factoring Examples. We illustrate the algorithm for $N = 15$ and 21. In the first simpler example of factoring $N = 15$, we proceed as follows. In a classical preprocessing step, we choose a

https://doi.org/10.1021/acs.jctc.3c00404
J. Chem. Theory Comput. 2023, 19, 6082−6092

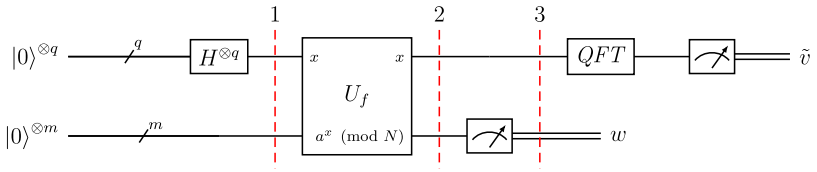

Figure 2. Quantum circuit for Shor's algorithm.

value for a that is coprime with 15 (say 2), calculate the needed number of qubits $q = 4$ and $m = 4$, and generate the modular exponentiation circuit for $f(x) = 2^x$ mod15 using adders and multipliers.[105] The execution of the quantum circuit proceeds as follows. The input register is initialized to the (unnormalized) equal superposition of $|0\rangle + |1\rangle + \cdots + |15\rangle$. At barrier (2), the two registers are entangled, producing the (unnormalized) state $|0\rangle|1\rangle + |1\rangle|2\rangle + |2\rangle|4\rangle + |3\rangle|8\rangle + |4\rangle|1\rangle + \cdots + |15\rangle|8\rangle$. A measurement of the output register may produce 1, 2, 4, or 8 with equal probability. Say we measure 4. The input register then collapses to the (unnormalized) state $|2\rangle + |6\rangle + |10\rangle + |14\rangle$. The QFT of this state is $|\tilde{0}\rangle + |\tilde{4}\rangle + |\tilde{8}\rangle + |\widetilde{12}\rangle$. Say we measure $|\widetilde{12}\rangle$. By properties of the QFT, we know that 12 is a multiple m of $16/s$, where s is the period we seek, i.e., $12m = 16/s$ or $12/16 = m/s$. The idea is that m/s is guaranteed to be a small irreducible fraction that approximates 12/16. In this case, we get the exact approximation 3/4, from which we infer that the period is 4. From the period, we calculate the two factors of 15 using gcd(15, $a^{s/2} \pm 1$), i.e., gcd(15, 3) = 3 and gcd(15, 5) = 5.

We follow the previous development with $N = 21$, $a = 10$, $q = 5$, and $m = 5$. At barrier (2), the (unnormalized) state is $|0\rangle|1\rangle + |1\rangle|10\rangle + |2\rangle|16\rangle + |3\rangle|13\rangle + |4\rangle|4\rangle + |5\rangle|19\rangle + |6\rangle|1\rangle + \cdots + |31\rangle|10\rangle$. Say we measure 13 at the output register. The input register collapses to the (unnormalized) state $|3\rangle + |9\rangle + \cdots + |27\rangle$. The QFT is not as perfect this time. We get the following distribution:

- $|\tilde{0}\rangle, |\widetilde{16}\rangle$ with probability 16%.
- $|\tilde{5}\rangle, |\widetilde{11}\rangle, |\widetilde{21}\rangle, |\widetilde{27}\rangle$ with probability 11%.
- other states with negligible probabilities.

Say we measure $|\widetilde{27}\rangle$. We know that $27m$ is close to $32/s$. Equivalently, we are looking for a small irreducible fraction close to 27/32. A classical calculation produces the approximation 5/6, yielding the period 6. From the period, we calculate gcd(21, $10^3 + 1$) = 7 and gcd(21, $10^3 - 1$) = 3.

3. MULTIPARTITE QUANTUM DYNAMICS AS TENSOR NETWORKS

The quantum algorithms of Section 2 and the tensor networks approach share some apparent similarities. In both cases, the systems are composed of multiple correlated parts that evolve quantum mechanically in a system-dependent manner and are interrogated using scenarios that measure one part of the system. This measurement affects the remaining parts of the system, whose spectral properties can then be inferred using the QFT. In this section, we make this intuitive correspondence precise, opening the door for richer connections between mathematically constructed algorithms and systems occurring in nature.

3.1. Multipartite Quantum Systems. We begin by considering a multidimensional quantum system represented as $A \oplus B$ composed of two correlated parts, A and B. Here, A and B can be multiple parts of a complex correlated quantum system,[63] or alternately, $A \oplus B$ can together represent a complex condensed-phase quantum dynamics problem,[77,78] where it may be more appropriate to refer to these as system and bath variables. The development here includes both descriptions. Such a system can be modeled in the tensor network formalism using a family of orthogonal states that represent subsystem A, referred to as $\{|\psi_i^A\rangle\}$, that may be correlated to (or entangled with) a family of mutually orthogonal states representing B and referred to as $\{|\psi_i^B\rangle\}$. The overall wave function is then written as a tensor product, or correlated sum, of the two components, namely,

$$|\psi\rangle = \sum_{i,j} C_{i,j} |\psi_i^A\rangle|\psi_j^B\rangle \tag{6}$$

The coefficients $C_{i,j}$ capture the degree to which the parts, A and B, are correlated to each other. For example, when $C_{i,j}$ is zero for all but one value of i and j, then A and B are completely decoupled, and a product approximation suffices. However, when this is not the case, the degree to which A and B influence each other is often important in physical systems. Another popular example of eq 6 are the well-known Bell states[6] for two-qubit systems, which are a sum of product states,

$$|\psi_{\text{Bell}}^1\rangle = \frac{1}{\sqrt{2}}[|0\rangle|1\rangle \pm |1\rangle|0\rangle] \tag{7}$$

or

$$|\psi_{\text{Bell}}^2\rangle = \frac{1}{\sqrt{2}}[|0\rangle|0\rangle \pm |1\rangle|1\rangle] \tag{8}$$

Equation 6 may also be rewritten using the Schmidt decomposition,[7] as

$$|\psi\rangle = \sum_i \alpha_i |\psi_i^A\rangle|\psi_i^B\rangle \tag{9}$$

which is essentially a bipartite matrix product state (MPS)[33] type tensor network[7,32] decomposition and is usually obtained by applying a sequence of singular value decomposition steps on the Tucker-form[7,106] of the entangled states in eq 6. Such states are common in quantum dynamics,[43,49,55,56,68,107] electronic structure,[32−35,43,108] and more recently, in quantum computing,[26] where the degree of correlation or entanglement between parts A and B are gauged using the $\{\alpha_i\}$-values. For the so-called maximally entangled states (such as Bell states and the Greenberger−Horne−Zeilinger (GHZ) states), α_i is a constant value for all i. (Compare eq 9 with eqs 7 and 8.) In quantum chemical dynamics, such highly correlated states are not common, and in general, the α_i-values may decay in some fashion when the sets of states $\{|\psi_i^A\rangle\}$ and $\{|\psi_i^B\rangle\}$ are appropriately ordered.

For a system containing $\mathcal{D}$ separate parts labeled as A_γ, $\gamma = 1 \cdots \mathcal{D}$, one may write the overall wave function in a form similar to eq 6:

$$|\psi\rangle = \sum_{i,j,\cdots} C_{i,j,\cdots,\mathcal{D}} |\psi_i^{A_1}\rangle|\psi_j^{A_2}\rangle\cdots|\psi_{\mathcal{D}}^{A_{\mathcal{D}}}\rangle \tag{10}$$

https://doi.org/10.1021/acs.jctc.3c00404
J. Chem. Theory Comput. 2023, 19, 6082−6092

where $C_{i,j,\cdots,\mathcal{D}}$ is a rank-$\mathcal{D}$ tensor and encodes the correlations between the constituents, $\{A_\gamma\}$. In fact, eq 10 is the starting point for the well-known multiconfigurational time-dependent Hartree (MCTDH) approach commonly used in multidimensional quantum dynamics[67,70,107] and vibrational spectroscopy.[70,92] The matrix product state representation of eq 10, obtained from a sequence of bipartite singular value decomposition steps, yields the MPS state

$$|\psi\rangle = \sum_{\bar{i}} |\psi_{i_1}^{A_1}\rangle\beta_{i_1}|\psi_{i_1,i_2}^{A_2}\rangle\beta_{i_2}\cdots\beta_{i_{\mathcal{D}-1}}|\psi_{i_{\mathcal{D}-1}}^{A_\mathcal{D}}\rangle$$
$$= \sum_{\bar{i}}\left[\prod_{\gamma=1}^{\mathcal{D}-1}\beta_{i_\gamma}\right]|\psi_{i_1}^{A_1}\rangle\left\{\prod_{\gamma=1}^{\mathcal{D}-2}|\psi_{i_\gamma,i_{\gamma+1}}^{A_\gamma}\rangle\right\}|\psi_{i_{\mathcal{D}-1}}^{A_\mathcal{D}}\rangle \tag{11}$$

where the coefficients $\{\beta_{i_\gamma}\}$ take on a generalization of the α_i in eq 9 and capture entanglement in a system with $\mathcal{D}$ parts.

3.2. Time Evolution of Multipartite Quantum Systems. In $A \oplus B$ systems occurring in quantum dynamics and electron−nuclear dynamics, we are often interested in learning about the influence of each part on the other. Toward this goal, without loss of generality, we begin by introducing an initial state of the $A \oplus B$ system that is an uncorrelated bipartite simplification of eq 9, that is,

$$|\psi_0\rangle = |\psi_0^A\rangle|\psi_0^B\rangle \tag{12}$$

The time evolution of the state $|\psi_0\rangle$ is given using a unitary evolution operator,

$$\mathcal{U}|\psi_0\rangle = \mathcal{U}|\psi_0^A\rangle|\psi_0^B\rangle \tag{13}$$

which may be further explicated by writing the time-evolution operator $\mathcal{U} \equiv \exp -\imath\mathcal{H}t/\hbar$ as a correlated matrix product operator[7,41,109,110] or a tensor product operator,

$$\mathcal{U} = \sum_\alpha \mathcal{U}_\alpha^A\mathcal{U}_\alpha^B \tag{14}$$

where, again, the multiple parts of the system are coupled by the overall Hamiltonian (and the time-evolution operator). Thus,

$$\mathcal{U}|\psi_0\rangle = \sum_\alpha [\mathcal{U}_\alpha^A|\psi_0^A\rangle][\mathcal{U}_\alpha^B|\psi_0^B\rangle] = \sum_\alpha |\phi_\alpha^A\rangle|\phi_\alpha^B\rangle \tag{15}$$

The structure of the Hamiltonian and the associated time-evolution operator result in the system correlations that are captured within the time-evolution process. This is represented by the sum of product states on the right side of eq 15. It must be noted here that while $\mathcal{U}$ is required to be unitary, in general, no such restrictions are present on $\{\mathcal{U}_\alpha^A; \mathcal{U}_\alpha^B\}$. This implies that while $|\phi_\alpha^A\rangle$ and $|\phi_\alpha^B\rangle$ may not, in general, be normalized, the overall propagated state is always normalized. For most physical systems, $\mathcal{U}$ has an explicit time dependence and is given by the exponential of a Hermitian operator as noted above, and hence $(|\phi_\alpha^A\rangle; |\phi_\alpha^B\rangle) \rightarrow (|\phi_\alpha^A(t)\rangle; |\phi_\alpha^B(t)\rangle)$. In such cases, the nonunitary nature of $\{\mathcal{U}_\alpha^A; \mathcal{U}_\alpha^B\}$, combined with the unitary nature of $\mathcal{U}$, yields a flow of probability between parts A and B. When only one term is present on the right side of eq 14, the two parts A and B are uncorrelated, and in such cases, $|\phi_\alpha^A(t)\rangle$ and $|\phi_\alpha^B(t)\rangle$ remain individually normalized, and there is no flow of information between the two parts.

Since the input states for each part of the system may be chosen from a complete set of states, $\{|\psi_i^A\rangle\}$ and $\{|\psi_i^B\rangle\}$, we may expand the final states, $|\phi_\alpha^A\rangle$ and $|\phi_\alpha^B\rangle$, using these as basis functions to obtain the general form of the composite state after time evolution as

$$\mathcal{U}|\psi_0\rangle = \sum_\alpha\left[\sum_j c_j^{A,\alpha}|\psi_j^A\rangle\right]\left[\sum_{j'} c_{j'}^{B,\alpha}|\psi_{j'}^B\rangle\right]$$
$$= \sum_{j,j'}\left[\sum_\alpha c_j^{A,\alpha}c_{j'}^{B,\alpha}\right]|\psi_j^A\rangle|\psi_{j'}^B\rangle \tag{16}$$

where $c_j^{A,\alpha} = \langle\psi_j^A|\mathcal{U}_\alpha^A|\psi_0^A\rangle$, and similarly for $c_j^{B,\alpha}$. Thus, it is the coefficient tensor, $\sum_\alpha c_j^{A,\alpha}c_{j'}^{B,\alpha}$ that builds in the correlations in eq 6 and is obtained here through time evolution by $\mathcal{U}$. At this stage, the two parts of the system are completely correlated to the extent allowed by the propagator $\mathcal{U}$. In fact, the extent of such a correlation may be precisely defined by the number of elements in the summation in eqs 14 and 16.

3.3. Final-State Analysis. At this stage in quantum chemical dynamics,[111] there are several analysis techniques available to gauge correlations within eq 16. There are two basic types of questions asked of the propagated state in eq 16. In one case, it is of interest to directly Fourier transform eq 16 in the time domain since these now provide the spectroscopic signatures of the Hamiltonian and, hence, the eigenspectrum of the Hamiltonian that governs the dynamics. This is common when only a few degrees of freedom are involved and tends to become prohibitive when the number of dimensions grow. Second, along the lines of the topic here, one is often interested in how the subsystem A evolves and is coupled to the properties of subsystem B. In a system-bath context, subsystem B may be considered as the bath degrees of freedom, whereas in a multidimensional quantum system or a reactive problem, subsystem B may contain modes that facilitate a chemical process or transition. This is a general problem and includes both condensed-phase quantum dynamics as well as electron−nuclear dynamics. It may also include chemical and biological sensing phenomena as signified by molecular binding processes.

Correspondingly, we project eq 16 onto a specific bath state $|\psi_k^B\rangle$, which is akin to performing a measurement on the bath state, to yield

$$\langle\psi_k^B|\mathcal{U}|\psi_0\rangle = \sum_j\left[\sum_\alpha c_j^{A,\alpha}c_k^{B,\alpha}\right]|\psi_j^A\rangle$$
$$= \sum_\alpha c_k^{B,\alpha}|\phi_\alpha^A\rangle \tag{17}$$

which represents the state after measurement on the bath state, with the measurement outcome

$$Tr[|\psi_k^B\rangle\langle\psi_k^B|\{\mathcal{U}|\psi_0\rangle\langle\psi_0|\mathcal{U}^\dagger\}] = Tr[|\langle\psi_k^B|\mathcal{U}|\psi_0\rangle|^2]$$
$$= Tr\left[\sum_{j,j'}\left[\sum_{\alpha,\alpha'} c_j^{A,\alpha}c_{j'}^{A,\alpha'*}c_k^{B,\alpha}c_k^{B,\alpha'*}\right]\{|\psi_j^A\rangle\langle\psi_{j'}^A|\}\right]$$
$$= Tr\left[\sum_{\alpha,\alpha'} c_k^{B,\alpha}c_k^{B,\alpha'*}|\phi_\alpha^A\rangle\langle\phi_{\alpha'}^A|\right]$$
$$= \sum_\alpha |c_k^{B,\alpha}|^2 \tag{18}$$

https://doi.org/10.1021/acs.jctc.3c00404
J. Chem. Theory Comput. 2023, 19, 6082−6092

Thus, while the result of measurement is the net probability of eq 16 along $|\psi_k^B\rangle$, that is eq 18, the remaining state is as in eq 17. A large number of such measurements on the bath state will yield various outcomes

$$\{Tr[|\langle\psi_j^B|\mathcal{U}|\psi_0\rangle|^2];\ |\psi_j^B\rangle\} \tag{19}$$

where each outcome, $|\langle\psi_j^B|\mathcal{U}|\psi_0\rangle|^2$, for bath state, $|\psi_j^B\rangle$, is accompanied by the system remaining in the state given in eq 17. In this manner, multiple measurements of B yield multiple states for A. Fourier transform of each of these yield,

$$\mathrm{FT}\left\{\sum_j\left[\sum_\alpha c_j^{A,\alpha}c_k^{B,\alpha}\right]|\psi_j^A\rangle\right\} = \mathrm{FT}\left\{\sum_\alpha c_k^{B,\alpha}|\phi_\alpha^A\rangle\right\} \tag{20}$$

essentially the state of A, and the degree of coupling, or entanglement, between the system (A) and bath (B) state as originally captured by eq 9. Equations 19 and 20 are critical to multiple areas of metrology in physical and biological sciences. In each case, the interpretation of systems A and B may be different. In sensing, an analyte might bind to system B, which collapses the system, and its Fourier transform (or a linear transform) may provide information about the analyte binding to B. Similar aspects exist in condensed-phase quantum dynamics and chemical catalysis as well.

3.4. Generalized Phase Kickback. In eq 18, part B is measured by using the same basis, $\{|\psi_k^B\rangle\}$, as that used for the original propagation. Suppose this was not the case and the measurement was done using a specific ket, $|\chi_k^B\rangle$ from within a different basis $\{|\chi_i^B\rangle\}$ where

$$|\chi_i^B\rangle = \sum_j d_{i,j}^B|\psi_j^B\rangle \tag{21}$$

and $d_{i,j}^B = \langle\psi_j^B|\chi_i^B\rangle$. In that case, eq 17, takes on a more general form:

$$\langle\chi_k^B|\mathcal{U}|\psi_0\rangle = \sum_{j,j'}\left[\sum_\alpha c_j^{A,\alpha}c_{j'}^{B,\alpha}\right]|\psi_j^A\rangle\langle\chi_k^B|\psi_{j'}^B\rangle$$

$$= \sum_{j,j'} d_{k,j'}^{B\,*}\left[\sum_\alpha c_j^{A,\alpha}c_{j'}^{B,\alpha}\right]|\psi_j^A\rangle \tag{22}$$

$$= \sum_{j',\alpha} d_{k,j'}^{B\,*}c_{j'}^{B,\alpha}|\phi_\alpha^A\rangle \tag{23}$$

(22)

Equation 23, as we show below, represents a generalized form of the phase kickback property, which is commonly seen in quantum information.[6] This can be illustrated by considering eqs 7 and 8 as our propagated states, $\mathcal{U}|\psi_0\rangle$. That is, to make a connection between the abstract tensor network formalism and qubits:

$$\{|\psi_i^A\rangle\} \rightarrow \{|0\rangle^A;\ |1\rangle^A\} \tag{24}$$

and similarly for B. Furthermore,

$$\{\mathcal{U}|\psi_0\rangle\} \rightarrow \{|\psi_{\mathrm{Bell}}^1\rangle;\ |\psi_{\mathrm{Bell}}^2\rangle\} \tag{25}$$

The measurement basis for phase kickback is chosen as

$$\{|\chi_i^B\rangle \rightarrow \{|+\rangle^B;\ |-\rangle^B\} \tag{26}$$

and therefore $d_{i,j}^B = \pm\,1/\sqrt{2}$ for all i,j. (See eq 21.) In that case, as per eq 23, when measurement is constructed using $|\pm^B\rangle$, one finds

$$\langle+^B|\psi_{\mathrm{Bell}}^1\rangle = \frac{1}{\sqrt{2}}|1\rangle^A \pm \frac{1}{\sqrt{2}}|0\rangle^A \tag{27}$$

and

$$\langle-^B|\psi_{\mathrm{Bell}}^1\rangle = \frac{1}{\sqrt{2}}|1\rangle^A \mp \frac{1}{\sqrt{2}}|0\rangle^A \tag{28}$$

That is, system A is rotated onto the X basis as a result of this measurement, or the phase angle in $\langle+^B|$is "kicked" into state A, upon measurement. Likewise,

$$\langle+^B|\psi_{\mathrm{Bell}}^2\rangle = \frac{1}{\sqrt{2}}|0\rangle^A \pm \frac{1}{\sqrt{2}}|1\rangle^A \tag{29}$$

and similarly $\langle-^B|\psi_{\mathrm{Bell}}^2\rangle$.

These features are captured in a general way within eqs 22 and 23, where the appropriate generalization of the phase kickback is in the terms $d_{k,j'}^{B\,*} \equiv \langle\chi_k^B|\psi_{j'}^B\rangle$ that represent the components of the measurement basis of B with respect to the initial basis and also the additional basis components that are "kicked-back" into system A, as per eq 22, after measurement on B.

The broader implications of eqs 22 and 23 are as follows: if we consider a general system containing two entangled parts, with the degree of entanglement dictated by a unitary evolution operator and hence an underlying Hamiltonian, a measurement or projection on one part, chosen as A here, is also noted in B. Thus, in some sense, B can "sense" the projection in A, but the extent of such a sensing process is dictated by the extent of entanglement present within $\mathcal{U}|\psi_0\rangle$ in eq 16. For the Bell state, the information is directly transferred, whereas for the state in eq 22, the measurement information is convoluted with the extent of entanglement.

4. CIRCUIT MODEL FOR MULTIPARTITE QUANTUM DYNAMICS

The development in the previous section can be recast in the circuit model to make the parallels with Shor's algorithm more explicit. We begin with Figure 3, which provides an instance of

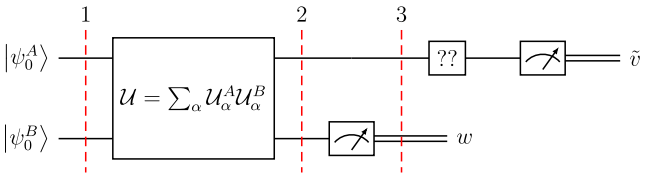

Figure 3. Quantum circuit version of bipartite quantum chemical dynamics problems. Beyond stage 3, the measurement box "??" signifies the fact that based on different measurements, connections between known quantum algorithms and chemical dynamics problems can be established.

the general formalism as a quantum circuit closely relating to the description of Shor's algorithm in Section 2. Specifically, the initial state in eq 12 is chosen to be a direct product state and represents Stage (1) in Figure 3. (Compare eqs 2 and 12.) It must be noted that this initial state, depicted at the end of Stage (1) in Figure 2, was obtained from a set of Hadamard transforms that essentially provide equal weights to all components of the computational basis embedded within the first wire stream of Figure 2.

https://doi.org/10.1021/acs.jctc.3c00404
J. Chem. Theory Comput. 2023, 19, 6082−6092

Thus, equivalently, A in Figure 3 may be entangled at Stage (1), but importantly, A and B are uncorrelated at this initial stage, and in this sense, eq 12 resembles the initial state for all of the quantum algorithms shown above. This state is then time-evolved as dictated by eq 14, leading to eqs 15 and 16, and is represented as Stage (2) in Figure 3. Similarly, the U_f operator in Figure 2 plays the same role as the propagator in Figure 3 and presents a correlated (or entangled) state, given by eq 3 and represented at Stage (2) in Figure 2. Following this time evolution leading to eqs 15 and 16, a measurement is constructed in all scenarios. We have presented only the analogue to Shor in Figure 3, complemented by the discussion in Section 3.3. The resultant state in Figure 3, given by eq 17, now represents a general and abstract interpretation of the resultant state of Shor's algorithm at Stage (3), prior to the QFT step.

The next step, as per Figures 2 and 3, is a Fourier transform of the state of the system, A, as described by eqs 19 and 20, which yields the momentum representation of the resultant state in subsystem A. In a sense, this also presents a more abstract form of the output from the top wire in Figure 2, and one may be induced to ask if we indeed obtain a similar "momentum representation" for the states captured in the top wire (natural numbers) in Figure 2. Thus, at the end of this process, if the Hamiltonian represented within the propagator in eq 14 (or in Shor's algorithm) entangles the A and B dimensions, then a measurement of B projects it onto a specific state. Following this, a Fourier transform of A yields the momentum representation and, in fact, the power spectrum of A for the specific projection of B.

Such a Fourier transform captures the entanglement within the composite $A \oplus B$ supersystem by probing the Fourier space structure of one part of the supersystem, namely, system A, for all possible measurement outcomes of system B (assuming that multiple measurements are done on B). For the specific choice of unitary in Shor's algorithm, this Fourier spectrum of A is always the same for any measurement of B. This may not, of course, be the case for naturally occurring or physicochemical systems.

Finally, we note a set of problems that may benefit from the analysis above. We will explore these connections in detail in future publications. Equation 6 resembles the total nonadiabatic electron−nuclear wave function[112−115] for molecular systems and may be written as an expansion in the complete set of electronic wave functions with the coefficients being functions of nuclear coordinates.[113] In multidimensional correlation spectroscopy,[116] vibrational mode coupling may be studied using similar partitioning schemes as in eq 6, where bath variables influence the dynamics of a chosen system. In fact, the example chosen in the next section is related to problems in multidimensional correlation spectroscopy.[117] In chemical catalysis, ligands that surround an active site may influence the reactive process. Such ideas are commonly used in catalyst design.[118] In chemical sensing of atmospheric and biological analytes, a perturbation to part A through a chemical binding process may result in a change in the state of B, given the extent of correlation in eq 6. In all such cases, one is always interested in the role that, for example, subsystem B in eq 6 plays in influencing the state of the remaining parts that are enclosed within A. The resulting analysis allows one to probe the correlations between subsystems A and B and has numerous practical applications in the set of examples.

5. APPLICATIONS: PROTONATED WATER WIRE SYSTEMS

We now exploit the formalism presented above to explore parallels between quantum algorithms and natural phenomena in physical, chemical, and biological systems.

Protonated water wires such as those in Figure 4a,b are encountered in a large variety of biological ion channels,

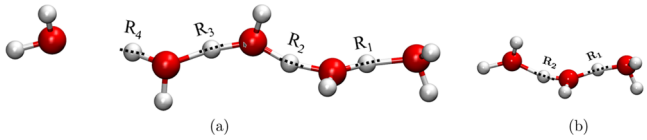

Figure 4. Protonated water wire with shared protons is treated quantum mechanically along the grid dimensions shown.

catalytic sites, light-harvesting systems, and fuel cells and form the central part of many condensed-phase chemical processes. Such systems are found in confined media such as ion channels. Quantum effects play a critical role in contributing to the rate of proton transport[119,120] and in determining vibrational properties.[88,121]

5.1. Coupled Stretch Modes in Protonated Water Dimer. In this section, we provide a tensor network description of such protonated systems, beginning with the simple case of two protons and extending to a longer water wire chain of multiple shared protons.

We begin with an analysis of the two shared proton dimensions marked as R_1 and R_2 in Figure 4b. Using the Schmidt decomposition,[7] the wave function for this two-dimensional system may be written as

$$\psi(x_1, x_2) = \sum_i \alpha_i \psi_i^1(x_1)\psi_i^2(x_2) \tag{30}$$

Here, $\{\psi_i^1(x_1)\}$ represents a family of functions that depicts the distribution of dimension R_1; this family is coupled to the family of functions, $\{\psi_i^2(x_2)\}$ that depicts the distribution of dimension R_2. Additionally, $\langle\psi_i^1|\psi_j^1\rangle = \langle\psi_i^2|\psi_j^2\rangle = \delta_{i,j}$ and thus these functions form an independent orthonormal basis for the two separate dimensions. For a $(H_2O)_3H^+$ water wire subsystem with degrees of freedom R_1 and R_2, the wave function components are calculated as shown in Figure 5a,b.

Several techniques can be used to investigate such systems. A basic one is to perform a measurement on one of the dimensions, say R_1. This interrogation could be done by projecting the system onto a specific state of R_1, say, $\psi_k^1(x_1)$. We then obtain

$$\langle\psi_k^1(x_1)|\psi(x_1, x_2)\rangle = \alpha_k\psi_k^2(x_2) \tag{31}$$

based on the orthogonality conditions stated above. The associated measurement outcome is

$$|\alpha_k|^2\|\psi_k^2\|^2 \tag{32}$$

and for $k = 1$, this quantity is close to 1, as indicated by the values of $\{\alpha_i\}$ provided in the caption for Figure 5.

More generally, we could also envision a more sophisticated measurement where the interrogation could be performed using the state $\chi^1(x_1) \equiv 1/\sqrt{2}[\psi_1^1(x_1) + \psi_2^1(x_1)]$ leading to a final state:

$$\langle\chi^1(x_1)|\psi(x_1, x_2)\rangle = \frac{1}{\sqrt{2}}[\alpha_1\psi_1^2(x_2) + \alpha_2\psi_2^2(x_2)] \tag{33}$$

https://doi.org/10.1021/acs.jctc.3c00404
J. Chem. Theory Comput. 2023, 19, 6082−6092

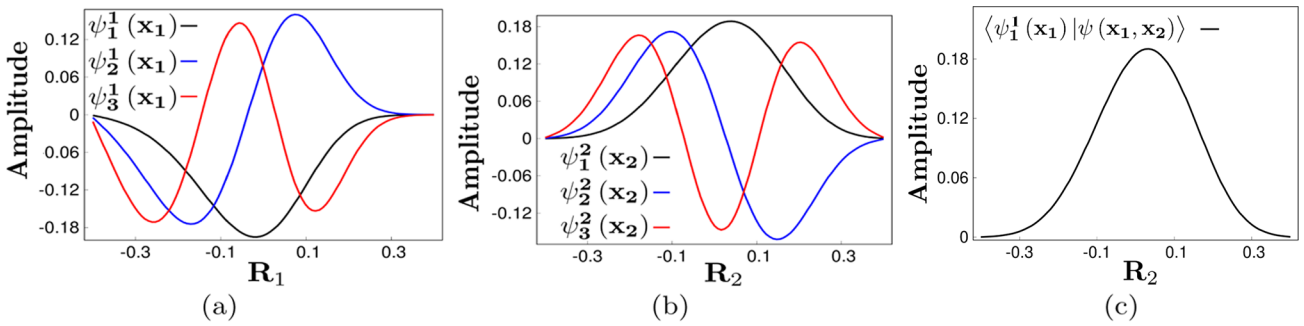

Figure 5. Figures (a) and (b) show functions $\{\psi_i^1(x_1)\}$ and $\{\psi_i^2(x_2)\}$ that form the state in eq 30, where $\alpha_1 = 0.9987$, $\alpha_2 = 0.0502$, and $\alpha_3 = 0.0022$. When measured with $\psi_1^1(x_2)$, one obtains Figure (c), with probability given by eq 31.

In this case, the superposition in the interrogation state is transferred to the outcome

$$\frac{1}{2}[|\alpha_1|^2\|\psi_1^2\|^2 + |\alpha_2|^2\|\psi_2^2\|^2] \approx 0.5 \tag{34}$$

In both interrogation scenarios, the measurement of one dimension influenced the other. Thus, the form of the state in eq 30 has a significant impact on the result of the observation. If one of the states that is already within the family included in eq 30 is used as the measurement basis, the outcome is the corresponding state within that family. However, when a combination of states is used as the measurement basis, the phase kickback mechanism causes the complex phase included in this combination to make its appearance in the measured outcome.

5.2. Coupled Stretch Modes in Protonated Water Pentamer. In biological systems, the water wire described above is often partially confined within an active site or inside an ion channel, as illustrated in Figure 6. In this section, we analyze an instance of such a system consisting of four degrees of freedom.

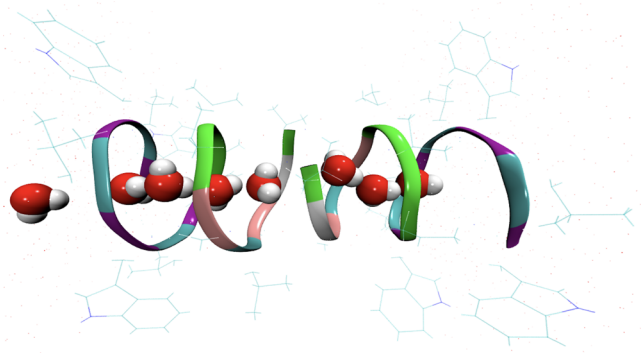

Figure 6. Water wire is confined within the Gramicidin ion channel.

Deferring the confinement modeling for a moment and focusing on the four degrees of freedom, the matrix product state for the coupled wave function has the form,

$$\psi(x_1, x_2, x_3, x_4) = \sum_{i_1,i_2,i_3} \psi_{i_1}^1(x_1)\alpha_{i_1}^1\psi_{i_1,i_2}^2(x_2)\alpha_{i_2}^2\psi_{i_2,i_3}^3(x_3)\alpha_{i_3}^3 \psi_{i_3}^4(x_4) \tag{35}$$

The quantities $\alpha_{i_j}^j$ in the equation above represent weights for the bond dimensions.

As we did in the previous section, we can model various interrogation scenarios. We show the result of performing a measurement on dimension R_1. This reduces eq 35 to produce

$$\langle\psi_k^1(x_1)|\psi(x_1, x_2, x_3, x_4)\rangle = \sum_{i_2,i_3} \alpha_k^1\psi_{k,i_2}^2(x_2)\alpha_{i_2}^2\psi_{i_2,i_3}^3(x_3)\alpha_{i_3}^3\psi_{i_3}^4(x_4) \tag{36}$$

and the corresponding measurement outcome is simply the magnitude of the vector in eq 36:

$$\langle\psi(x_1, x_2, x_3, x_4)|\psi_k^1(x_1)\rangle\langle\psi_k^1(x_1)|\psi(x_1, x_2, x_3, x_4)\rangle \tag{37}$$

This simple analysis ignored the fact that in most biological systems (especially ion channels as well as enzyme active sites), the water molecules that encapsulate dimensions R_2 and R_3 have a limited degree of flexibility. This results in a limited degree of projection of dimensions R_2 and R_3 into, for example, a subspace given by

$$\chi_k(x_2, x_3) \equiv \sum_{i_2,i_3} \beta_{i_2,i_3}\psi_{k,i_2}^2(x_2)\psi_{i_2,i_3}^3(x_3) \tag{38}$$

Note that such a state is not dissimilar to the measurement basis state used in the phase kickback scenario at the end of Section 3 and reduces the possible outcomes for x_4. Thus, after projection of eq 38 onto eq 36, we obtain

$$\sum_{i_2,i_3} (\beta_{i_2,i_3}\alpha_k^1\alpha_{i_2}^2\alpha_{i_3}^3)\psi_{i_3}^4(x_4) \tag{39}$$

where the bracketed set acts as a combined coefficient that curtails the set of possibilities for x_4. Thus, based on the extent of flexibility provided by the restrictions to β_{i_2,i_3}, there are a range of possible outcomes at the far end depicted by x_4.

This idea can be generalized for an arbitrary number of degrees of freedom, where, using eq 39, we may write our final result as

$$\sum_{i_2,\cdots,i_{N-1}} (\beta_{i_2,\cdots,i_{N-1}}\alpha_k^1\alpha_{i_2}^2\cdots\alpha_{i_{N-1}}^{N-1})\psi_{i_{N-1}}^N(x_N) \tag{40}$$

5.3. Circuit Model for Protonated Water Wire. We now analyze the results from the two sections above using the quantum circuit model. The quantum circuits thus derived are based on Figure 3 and are presented in Figures 7 and 8. As discussed in Section 4, all parts of both systems are correlated at the end of Stage (2) with wave functions given by eqs 30 and 35. In the case of the protonated water dimer, a measurement along dimension R_1 follows, resulting in the projected state given by eq

https://doi.org/10.1021/acs.jctc.3c00404
J. Chem. Theory Comput. 2023, 19, 6082−6092

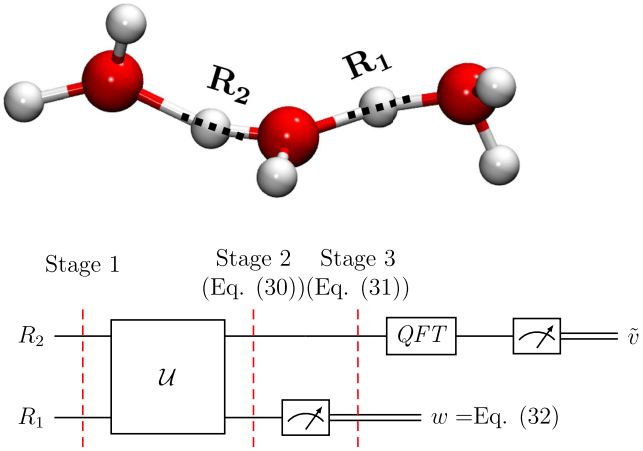

Figure 7. Quantum circuit version for protonated water-dimer system is discussed in Section 5.1.

31 at Stage (3), with the measurement probability given by eq 32.

The protonated pentamer problem is complicated due to the phase kickback step resulting from basis rotations (eq 39 on the (R_2, R_3) degrees of freedom, as shown in Figure 8). Specifically, the correlated state at Stage (2) given by eq 35 undergoes measurements at R_1, with the outcome, eq 37, where the corresponding resultant state is then projected onto a rotated basis within dimensions R_2 and R_3, given by eq 38 to arrive at Stage (3) at the state given by eq 39. Thus, Figures 7 and 8, through the discussion accompanying Figure 3, provide a detailed analogue to the Shor algorithm in Figure 2 by way of an abstract formalism presented in Section 3.

6. CONCLUSIONS

In this article, we have developed an abstract formalism of tensor network-based quantum dynamics applicable broadly for all quantum systems, and we discuss how this general idea captures the key signatures within the well-known Shor's algorithm as well as other well-known quantum algorithms. In essence, for a general bipartite system, unitary evolution encodes within the evolved state a characteristic correlation or entanglement that bears the signature of the Hamiltonian that defines the evolution operator. Thus, once we interrogate a specific part of a quantum system, the remaining parts of that system automatically get projected based on the extent of correlation that resides within the system, and this is borne out of measurement.

This close resemblance of the general formalism of quantum propagation of multipartite systems and the symmetry of integers as captured by Shor's algorithm begs the rather profound question of whether natural systems exist or can be designed that may perform the operations that we might interpret as prime-factoring. We do not dwell on this general question in this article, but we ask the opposite question of whether we can exploit this connection to analyze quantum chemical dynamics. Indeed, we find that when we apply this concept along with the generalized definition of phase kickback as obtained from the tensor network description of Shor's algorithm and quantum dynamics described here, the coupled dynamics of protons in a protonated water wire naturally lends itself to a projected transport interpretation. We find that projection of states at one end of a water wire, along with phase kickback-like constrained operations along the length of the water chain, provide a general description for proton transport that is commensurate with our description of Shor's algorithm. Future publications are currently planned to exploit this analogy to probe electron−nuclear dynamics in the nonadiabatic setting. Furthermore, given that the surrounding vibrational degrees of freedom may be projected through phase kickback, as noted here, to tailor the dynamics within one mode (R_4 for the protonated pentamer), perhaps chemical catalysis is another area where these broad ideas may find application. These aspects will be probed in future work.

AUTHOR INFORMATION

Corresponding Authors

Srinivasan S. Iyengar − *Department of Chemistry, Indiana University, Bloomington, Indiana 47405-7102, United States; Quantum Science and Engineering Center (QSEc), Indiana*

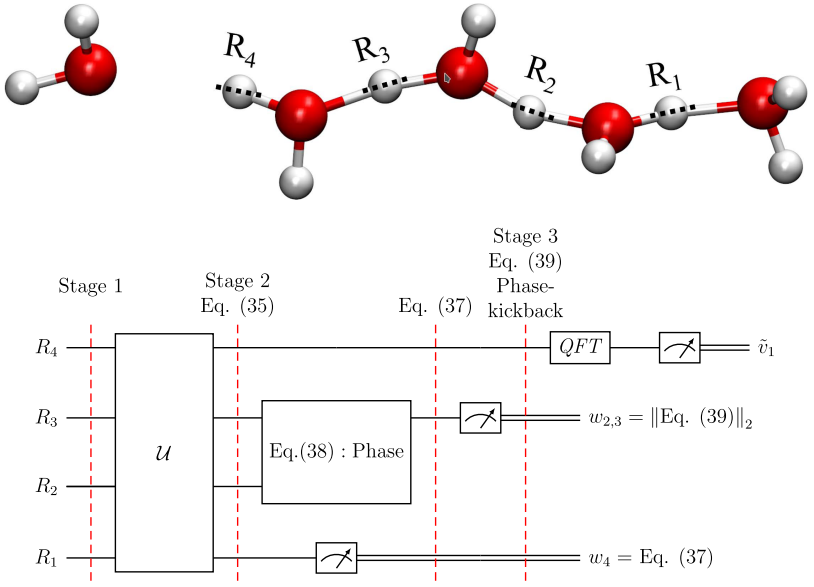

Figure 8. Quantum circuit version for protonated water-pentamer system is discussed in Section 5.2. A combination of a simple measurement at R_1, given by eqs 36 and 37 and a rotation for R_2,R_3, given by eq 39 and its norm results in a composite final outcome at Stage 3 for R_4.

https://doi.org/10.1021/acs.jctc.3c00404
J. Chem. Theory Comput. 2023, 19, 6082−6092

University, Bloomington, Indiana 47405-7102, United States; orcid.org/0000-0001-6526-2907; Email: iyengar@indiana.edu

Amr Sabry − *Quantum Science and Engineering Center (QSEc) and Department of Computer Science, Luddy School of Informatics, Computing, and Engineering, Indiana University, Bloomington, Indiana 47405-7102, United States;* Email: sabry@indiana.edu

Authors

Anup Kumar − *Department of Chemistry, Indiana University, Bloomington, Indiana 47405-7102, United States*

Debadrita Saha − *Department of Chemistry, Indiana University, Bloomington, Indiana 47405-7102, United States*

Complete contact information is available at: https://pubs.acs.org/10.1021/acs.jctc.3c00404

Notes

The authors declare no competing financial interest.

■ ACKNOWLEDGMENTS

This research was supported by the National Science Foundation grants OMA-1936353 to authors S.S.I. and A.S., and CHE-2102610 to S.S.I.

■ REFERENCES

(1) Preskill, J. Quantum Computing in the NISQ era and beyond. *Quantum* **2018**, *2*, 79.
(2) McArdle, S.; Endo, S.; Aspuru-Guzik, A.; Benjamin, S. C.; Yuan, X. Quantum computational chemistry. *Rev. Mod. Phys.* **2020**, *92*, No. 015003.
(3) Cao, Y.; Romero, J.; Olson, J. P.; Degroote, M.; Johnson, P. D.; Kieferová, M.; Kivlichan, I. D.; Menke, T.; Peropadre, B.; Sawaya, N. P. D.; Sim, S.; Veis, L.; Aspuru-Guzik, A. Quantum Chemistry in the Age of Quantum Computing. *Chem. Rev.* **2019**, *119*, 10856−10915.
(4) Aspuru-Guzik, A.; Dutoi, A. D.; Love, P. J.; Head-Gordon, M. Simulated quantum computation of molecular energies. *Science* **2005**, *309*, 1704.
(5) Shor, P. W. Polynomial-Time Algorithms for Prime Factorization and Discrete Logarithms on a Quantum Computer. *SIAM J. Comput.* **1997**, *26*, 1484−1509.
(6) Nielsen, M. A.; Chuang, I. L. *Quantum Computation and Quantum Information*; Cambridge University Press, New York, NY, USA, 2000.
(7) Orús, R. A practical introduction to tensor networks: Matrix product states and projected entangled pair states. *Ann. Phys.* **2014**, *349*, 117−158.
(8) Oseledets, I. V. Tensor-Train Decomposition. *SIAM J. Sci. Comput.* **2011**, *33*, 2295−2317.
(9) Kolda, T. G.; Bader, B. W. Tensor Decompositions and Applications. *SIAM Rev.* **2009**, *51*, 455−500.
(10) De Lathauwer, L.; De Moor, B.; Vandewalle, J. A Multilinear Singular Value Decomposition. *SIAM J. Matrix Anal. Appl.* **2000**, *21*, 1253−1278.
(11) Kanjilal, P. P.; Palit, S.; Saha, G. Fetal ECG extraction from single-channel maternal ECG using singular value decomposition. *IEEE Trans. Biomed. Eng.* **1997**, *44*, 51−59.
(12) Rajwade, A.; Rangarajan, A.; Banerjee, A. Image Denoising Using the Higher Order Singular Value Decomposition. *IEEE Trans. Pattern Anal. Mach. Intell.* **2013**, *35*, 849−862.
(13) Iqbal, N.; Zerguine, A.; Kaka, S.; Al-Shuhail, A. Automated SVD filtering of time-frequency distribution for enhancing the SNR of microseismic/microquake events. *J. Geophys. Eng.* **2016**, *13*, 964.
(14) Hu, C.; Lu, X.; Ye, M.; Zeng, W. Singular value decomposition and local near neighbors for face recognition under varying illumination. *Pattern Recognit.* **2017**, *64*, 60−83.
(15) Verstraete, F.; Murg, V.; Cirac, J. I. Matrix product states, projected entangled pair states, and variational renormalization group methods for quantum spin systems. *Adv. Phys.* **2008**, *57*, 143−224.
(16) Bridgeman, J. C.; Chubb, C. T. Hand-waving and interpretive dance: an introductory course on tensor networks. *J. Phys. A: Math. Theor.* **2017**, *50*, No. 223001.
(17) Montangero, S. *Introduction to Tensor Network Methods: Numerical Simulations of Low-Dimensional Many-Body Quantum Systems*; Springer: Cham, 2018.
(18) Ran, S.-J.; Tirrito, E.; Peng, C.; Chen, X.; Tagliacozzo, L.; Su, G.; Lewenstein, M. *Tensor Network Contractions: Methods and Applications to Quantum Many-Body Systems*; Springer: Cham, 2020.
(19) Silvi, P.; Tschirsich, F.; Gerster, M.; Jünemann, J.; Jaschke, D.; Rizzi, M.; Montangero, S. The Tensor Networks Anthology: Simulation techniques for many-body quantum lattice systems. *SciPost Phys. Lect. Notes* **2019**, *8*, No. 008, DOI: 10.21468/SciPostPhysLectNotes.8.
(20) Orús, R. Tensor networks for complex quantum systems. *Nat. Rev. Phys.* **2019**, *1*, 538−550.
(21) Orús, R. A practical introduction to tensor networks: Matrix product states and projected entangled pair states. *Ann. Phys.* **2014**, *349*, 117−158.
(22) Biamonte, J.; Bergholm, V. Tensor Networks in a Nutshell. 2017, arXiv:1708.00006. arXiv.org e-Print archive. http://arxiv.org/abs/1708.00006.
(23) Biamonte, J. Lectures on Quantum Tensor Networks. 2019, arXiv:1912.10049. arXiv.org e-Print archive. http://arxiv.org/abs/1912.10049.
(24) Eisert, J. Entanglement and Tensor Network States. 2013, arXiv:1308.3318. arXiv.org e-Print archive. http://arxiv.org/abs/1308.3318.
(25) Wood, C. J.; Biamonte, J. D.; Cory, D. G. Tensor Networks and Graphical Calculus for Open Quantum Systems. 2015, arXiv:1111.6950. arXiv.org e-Print archive. http://arxiv.org/abs/1111.6950.
(26) Peng, T.; Harrow, A. W.; Ozols, M.; Wu, X. Simulating Large Quantum Circuits on a Small Quantum Computer. *Phys. Rev. Lett.* **2020**, *125*, No. 150504.
(27) Fried, E. S.; Sawaya, N. P. D.; Cao, Y.; Kivlichan, I. D.; Romero, J.; Aspuru-Guzik, A. qTorch: The quantum tensor contraction handler. *PLoS One* **2018**, *13*, No. e0208510.
(28) Schutski, R.; Lykov, D.; Oseledets, I. Adaptive algorithm for quantum circuit simulation. *Phys. Rev. A* **2020**, *101*, No. 042335.
(29) Bauer, B.; Bravyi, S.; Motta, M.; Kin-Lic Chan, G. Quantum Algorithms for Quantum Chemistry and Quantum Materials Science. *Chem. Rev.* **2020**, *120*, 12685−12717.
(30) Hastings, M. B. An area law for one-dimensional quantum systems. *J. Stat. Mech.: Theory Exp.* **2007**, *2007*, No. P08024.
(31) Eisert, J.; Cramer, M.; Plenio, M. B. Colloquium: Area laws for the entanglement entropy. *Rev. Mod. Phys.* **2010**, *82*, 277−306.
(32) White, S. R. Density matrix formulation for quantum renormalization groups. *Phys. Rev. Lett.* **1992**, *69*, 2863−2866.
(33) Schollwöck, U. The density-matrix renormalization group in the age of matrix product states. *Ann. Phys.* **2011**, *326*, 96−192.
(34) Schollwöck, U. The density-matrix renormalization group. *Rev. Mod. Phys.* **2005**, *77*, 259−315.
(35) Keller, S. F.; Reiher, M. Determining Factors for the Accuracy of DMRG in Chemistry. *CHIMA Int. J. Chem.* **2014**, *68*, 200−203.
(36) Hastings, M. B. Solving gapped Hamiltonians locally. *Phys. Rev. B* **2006**, *73*, No. 085115.
(37) Vidal, G. Classical simulation of infinite-size quantum lattice systems in one spatial dimension. *Phys. Rev. Lett.* **2007**, *98*, No. 070201.
(38) Haegeman, J.; Cirac, J. I.; Osborne, T. J.; Pižorn, I.; Verschelde, H.; Verstraete, F. Time-dependent variational principle for quantum lattices. *Phys. Rev. Lett.* **2011**, *107*, No. 070601.
(39) Vidal, G. Efficient simulation of one-dimensional quantum many-body systems. *Phys. Rev. Lett.* **2004**, *93*, No. 040502.
(40) Szalay, S.; Pfeffer, M.; Murg, V.; Barcza, G.; Verstraete, F.; Schneider, R.; Legeza, O. Tensor product methods and entanglement

optimization for ab initio quantum chemistry. *Int. J. Quantum Chem.* **2015**, *115*, 1342−1391.
(41) Chan, G. K.-L.; Keselman, A.; Nakatani, N.; Li, Z.; White, S. R. Matrix product operators, matrix product states, and ab initio density matrix renormalization group algorithms. *J. Chem. Phys.* **2016**, *145*, No. 014102.
(42) Gunst, K.; Verstraete, F.; Wouters, S.; Legeza, O.; Van Neck, D. T3NS: Three-Legged Tree Tensor Network States. *J. Chem. Theory Comput.* **2018**, *14*, 2026−2033.
(43) Kumar, A.; DeGregorio, N.; Ricard, T.; Iyengar, S. S. Graph-Theoretic Molecular Fragmentation for Potential Surfaces Leads Naturally to a Tensor Network Form and Allows Accurate and Efficient Quantum Nuclear Dynamics. *J. Chem. Theory Comput.* **2022**, *18*, 7243.
(44) Daul, S.; Ciofini, I.; Daul, C.; White, S. R. Full-CI quantum chemistry using the density matrix renormalization group. *Int. J. Quantum Chem.* **2000**, *79*, 331−342.
(45) Mitrushenkov, A. O.; Fano, G.; Ortolani, F.; Linguerri, R.; Palmieri, P. Quantum chemistry using the density matrix renormalization group. *J. Chem. Phys.* **2001**, *115*, 6815−6821.
(46) Mitrushenkov, A. O.; Linguerri, R.; Palmieri, P.; Fano, G. Quantum chemistry using the density matrix renormalization group II. *J. Chem. Phys.* **2003**, *119*, 4148−4158.
(47) Chan, G. K.-L. An algorithm for large scale density matrix renormalization group calculations. *J. Chem. Phys.* **2004**, *120*, 3172−3178.
(48) Chan, G. K.-L.; Kállay, M.; Gauss, J. State-of-the-art density matrix renormalization group and coupled cluster theory studies of the nitrogen binding curve. *J. Chem. Phys.* **2004**, *121*, 6110−6116.
(49) Baiardi, A.; Stein, C. J.; Barone, V.; Reiher, M. Vibrational Density Matrix Renormalization Group. *J. Chem. Theory Comput.* **2017**, *13*, 3764−3777.
(50) Baiardi, A.; Reiher, M. Large-scale quantum dynamics with matrix product states. *J. Chem. Theory Comput.* **2019**, *15*, 3481−3498.
(51) Baiardi, A.; Stein, C. J.; Barone, V.; Reiher, M. Optimization of highly excited matrix product states with an application to vibrational spectroscopy. *J. Chem. Phys.* **2019**, *150*, No. 094113.
(52) Rakhuba, M.; Oseledets, I. Calculating vibrational spectra of molecules using tensor train decomposition. *J. Chem. Phys.* **2016**, *145*, No. 124101.
(53) Glaser, N.; Baiardi, A.; Reiher, M. *Vibrational Dynamics of Molecules*; World Scientific, 2021; pp 80−144.
(54) Baranov, V.; Oseledets, I. Fitting high-dimensional potential energy surface using active subspace and tensor train (AS+TT) method. *J. Chem. Phys.* **2015**, *143*, No. 174107.
(55) DeGregorio, N.; Iyengar, S. S. Adaptive Dimensional Decoupling for Compression of Quantum Nuclear Wave Functions and Efficient Potential Energy Surface Representations through Tensor Network Decomposition. *J. Chem. Theory Comput.* **2019**, *15*, 2780−2796.
(56) Greene, S. M.; Batista, V. S. Tensor-Train Split-Operator Fourier Transform (TT-SOFT) Method: Multidimensional Nonadiabatic Quantum Dynamics. *J. Chem. Theory Comput.* **2017**, *13*, 4034−4042.
(57) Schlimgen, A. W.; Head-Marsden, K.; Sager-Smith, L. M.; Narang, P.; Mazziotti, D. A. Quantum Simulation of Open Quantum Systems Using Density-Matrix Purification. 2022, arXiv:2207.07112. arXiv.org e-Print archive. http://arxiv.org/abs/2207.07112.
(58) Sulz, D.; Lubich, C.; Ceruti, G.; Lesanovsky, I.; Carollo, F. Numerical Simulations of Long-Range Open Quantum Many-Body Dynamics with Tree Tensor Networks. 2023, arXiv:2304.06075. arXiv.org e-Print archive. http://arxiv.org/abs/2304.06075.
(59) Hassanpour, H. A time-frequency approach for noise reduction. *Digit. Signal Process.* **2008**, *18*, 728−738.
(60) Liu, Y.; Li, W.-J.; Zhang, X.; Lewenstein, M.; Su, G.; Ran, S.-J. Entanglement-Based Feature Extraction by Tensor Network Machine Learning. *Front. Appl. Math. Stat.* **2021**, *7*, No. 716044, DOI: 10.3389/fams.2021.716044.
(61) Liu, J.; Li, S.; Zhang, J.; Zhang, P. Tensor networks for unsupervised machine learning. *Phys. Rev. E* **2021**, *107*, No. L012103, DOI: 10.1103/PhysRevE.107.L012103.
(62) Stoudenmire, E.; Schwab, D. J. Supervised learning with tensor networks. *Adv. Neural Inf. Process. Syst.* **2016**, *29*, 4806−4814.
(63) *Dynamics of Molecules and Chemical Reactions*, Wyatt, R. E.; Zhang, J. Z. H., Eds.; Marcel Dekker Inc: New York, NY, 1996.
(64) Peng, T.; Zhang, J. Z. H. A Reactant-Product Decoupling Method for State-To-State Reactive Scattering. *J. Chem. Phys.* **1996**, *105*, 6072.
(65) Althorpe, S. C.; Clary, D. C. Quantum Scattering Calculations on Chemical Reactions. *Annu. Rev. Phys. Chem.* **2003**, *54*, 493.
(66) Bowman, J. M. The Self-Consistent-Field Approach to Polyatomic Vibrations. *Acc. Chem. Res.* **1986**, *19*, 202.
(67) Meyer, H.-D.; Manthe, U.; Cederbaum, L. S. The multi-configurational time-dependent Hartree approach. *Chem. Phys. Lett.* **1990**, *165*, 73−78.
(68) Binder, R.; Burghardt, I. First-principles quantum simulations of exciton diffusion on a minimal oligothiophene chain at finite temperature. *Faraday Discuss.* **2020**, *221*, 406−427.
(69) Wang, H.; Thoss, M. Multilayer formulation of the multi-configuration time-dependent Hartree theory. *J. Chem. Phys.* **2003**, *119*, 1289−1299.
(70) Wodraszka, R.; Carrington, T. Systematically expanding nondirect product bases within the pruned multi-configuration time-dependent Hartree (MCTDH) method: A comparison with multi-layer MCTDH. *J. Chem. Phys.* **2017**, *146*, No. 194105.
(71) Iyengar, S. S.; Jakowski, J. Quantum Wavepacket Ab Initio Molecular Dynamics: An Approach to Study Quantum Dynamics in Large Systems. *J. Chem. Phys.* **2005**, *122*, No. 114105.
(72) Kadanoff, L. P.; Baym, G. *Quantum Statistical Mechanics. Green's Function Methods in Equilibrium Problems*; W. A. Benjamin: New York, 1962.
(73) Mujica, V.; Kemp, M.; Ratner, M. A. Electron Conduction in Molecular Wires. I. a Scattering Formalism. *J. Chem. Phys.* **1994**, *101*, 6849.
(74) Mujica, V.; Kemp, M.; Ratner, M. A. Electron Conduction in Molecular Wires. II. Application to Scanning Tunneling Microscopy. *J. Chem. Phys.* **1994**, *101*, 6856.
(75) Datta, S. *Quantum Transport Atom to Transistor*; Cambridge University Press, 2005.
(76) Xue, Y. Q.; Datta, S.; Ratner, M. A. First-Principles Based Matrix Green's Function Approach to Molecular Electronic Devices: General Formalism. *Chem. Phys.* **2002**, *281*, 151.
(77) Caldeira, A. O.; Leggett, A. J. Quantum tunnelling in a dissipative system. *Ann. Phys.* **1983**, *149*, 374−456.
(78) Leggett, A. J.; Chakravarty, S.; Dorsey, A. T.; Fisher, M. P. A.; Garg, A.; Zwerger, W. Dynamics of the dissipative two-state system. *Rev. Mod. Phys.* **1987**, *59*, 1−85.
(79) Yuen-Zhou, J.; Tempel, D. G.; Rodríguez-Rosario, C. A.; Aspuru-Guzik, A. Time-Dependent Density Functional Theory for Open Quantum Systems with Unitary Propagation. *Phys. Rev. Lett.* **2010**, *104*, No. 043001.
(80) Galperin, M.; Nitzan, A. Negf-Hf Method in Molecular Junction Property Calculations. *Ann. N.Y. Acad. Sci.* **2003**, *1006*, 48.
(81) Pacheco, A. B.; Iyengar, S. S. A Multi-Stage Ab-Initio Quantum Wavepacket Dynamics Formalism for Electronic Structure and Dynamics in Open Systems. *J. Chem. Phys.* **2010**, *133*, No. 044105.
(82) Pacheco, A. B.; Iyengar, S. S. Multi-Stage Ab-Initio Quantum Wavepacket Dynamics for Electronic Structure and Dynamics in Open Systems: Momentum Representation, Coupled Electron Nuclear Dynamics and External Fields. *J. Chem. Phys.* **2011**, *134*, No. 074107.
(83) Shannon, C. E. A Mathematical Theory of Communication. *Bell Syst. Tech. J.* **1948**, *27*, 279.
(84) Vedral, V. *Decoding Reality: The Universe as Quantum Information*; Oxford University Press: New York, 2010.
(85) Gleick, J. *The Information: A History, A Theory, A Flood*; Pantheon/Random House: New York, 2011.
(86) Ball, P. Physics of life: The dawn of quantum biology. *Nature* **2011**, *474*, 272.
(87) Deutsch, D. *The Fabric of Reality*; Penguin, 1997.

(88) Shin, J.-W.; Hammer, N. I.; Diken, E. G.; Johnson, M. A.; Walters, R. S.; Jaeger, T. D.; Duncan, M. A.; Christie, R. A.; Jordan, K. D. Infrared Signature of Structures Associated with the $H^+(H_2O)_n$ (N = 6 to 27) Clusters. *Science* **2004**, *304*, 1137.
(89) Hammer, N. I.; Diken, E. G.; Roscioli, J. R.; Johnson, M. A.; Myshakin, E. M.; Jordan, K. D.; McCoy, A. B.; Huang, X.; Bowman, J. M.; Carter, S. The Vibrational Predissociation Spectra of the $H_5O_2^+ \cdot RG_n$(RG = Ar,Ne) clusters: Correlation of the solvent perturbations in the free OH and shared proton transitions of the Zundel ion. *J. Chem. Phys.* **2005**, *122*, No. 244301.
(90) Fournier, J. A.; Wolke, C. T.; Johnson, M. A.; Odbadrakh, T. T.; Jordan, K. D.; Kathmann, S. M.; Xantheas, S. S. Snapshots of Proton Accommodation at a Microscopic Water Surface: Understanding the Vibrational Spectral Signatures of the Charge Defect in Cryogenically Cooled $H(H_2O)_n^+$= 2−28 Clusters. *J. Phys. Chem. A* **2015**, *119*, 37.
(91) Headrick, J. M.; Diken, E. G.; Walters, R. S.; Hammer, N. I.; Christie, R. A.; Cui, J.; Myshakin, E. M.; Duncan, M. A.; Johnson, M. A.; Jordan, K. Spectral Signatures of Hydrated Proton Vibrations in Water Clusters. *Science* **2005**, *308*, 1765.
(92) Vendrell, O.; Gatti, F.; Meyer, H.-D. Dynamics and Infrared Spectroscopy of the Protonated Water Dimer. *Angew. Chem., Int. Ed.* **2007**, *46*, 6918.
(93) Vendrell, O.; Meyer, H. D. Proton Conduction Along a Chain of Water Molecules. Development of a Linear Model and Quantum Dynamical Investigations Using the Multiconfiguration Time-Dependent Hartree Method. *J. Chem. Phys.* **2005**, *122*, No. 104505.
(94) Drukker, K.; Hammes-Schiffer, S. An Analytical Derivation of MC-SCF Vibrational Wave Functions for the Quantum Dynamical Simulation of Multiple Proton Transfer Reactions: Initial Application to Protonated Water Chains. *J. Chem. Phys.* **1997**, *107*, 363.
(95) Bernstein, E.; Vazirani, U. Quantum Complexity Theory. *SIAM J. Comput.* **1997**, *26*, 1411−1473.
(96) Deutsch, D. Quantum theory, the Church-Turing principle and the universal quantum computer. *Proc. R. Soc. London, Ser. A* **1985**, *400*, 97−117.
(97) Deutsch, D.; Jozsa, R. Rapid solution of problems by quantum computation. *Proc. R. Soc. London, Ser. A* **1992**, *439*, 553−558.
(98) Simon, D. R. In *On the Power of Quantum Computation*, Proceedings 35th Annual Symposium on Foundations of Computer Science, 1994; pp 116−123.
(99) Simon, D. R. On the Power of Quantum Computation. *SIAM J. Comput.* **1997**, *26*, 1474−1483.
(100) Shor, P. W. Polynomial-Time Algorithms for Prime Factorization and Discrete Logarithms on a Quantum Computer. *SIAM J. Comput.* **1997**, *26*, 1484−1509.
(101) Nielsen, M. A.; Chuang, I. L. *Quantum Computation and Quantum Information*; Cambridge University Press, 2010.
(102) Grover, L. K. In *A Fast Quantum Mechanical Algorithm for Database Search*, Proceedings of the Twenty-Eighth Annual ACM Symposium on Theory of Computing. New York, NY, USA, 1996; pp 212−219.
(103) Coppersmith, D. An Approximate Fourier Transform Useful in Quantum Factoring. 2002, arXiv:0201067. arXiv.org e-Print archive. http://arxiv.org/abs/0201067.
(104) Dumitrescu, E. Tree tensor network approach to simulating Shor's algorithm. *Phys. Rev. A* **2017**, *96*, No. 062322.
(105) Vedral, V.; Barenco, A.; Ekert, A. Quantum networks for elementary arithmetic operations. *Phys. Rev. A* **1996**, *54*, 147−153.
(106) Tucker, L. R. The Extension of Factor Analysis to Three-Dimensional Matrices. In *Contributions to Mathematical Psychology*; Gulliksen, H.; Frederiksen, N., Eds.; Rinehart & Winston: Winston, NY, 1964; pp 109−127.
(107) Otto, F. Multi-layer Potfit: An accurate potential representation for efficient high-dimensional quantum dynamics. *J. Chem. Phys.* **2014**, *140*, No. 014106.
(108) Peláez, D.; Meyer, H.-D. The multigrid POTFIT (MGPF) method: Grid representations of potentials for quantum dynamics of large systems. *J. Chem. Phys.* **2013**, *138*, No. 014108.
(109) García-Ripoll, J. J. Time evolution of matrix product states. *New J. Phys.* **2006**, *8*, 305.
(110) Pirvu, B.; Murg, V.; Cirac, J. I.; Verstraete, F. Matrix product operator representations. *New J. Phys.* **2010**, *12*, No. 025012.
(111) Newton, R. G. *Scattering Theory of Waves and Particles*; Springer-Verlag: New York, 1982.
(112) Tully, J. C. Molecular Dynamics with Electronic Transitions. *J. Chem. Phys.* **1990**, *93*, 1061.
(113) Coker, D. F. *Computer Simulation in Chemical Physics*, Tildesley, D. J., Ed.; Kluwer Academic Publishers: Dordrecht, The Netherlands, 1993.
(114) Skone, J. H.; Pak, M. V.; Hammes-Schiffer, S. Nuclear-Electronic Orbital Nonorthogonal Configuration Interaction Approach. *J. Chem. Phys.* **2005**, *123*, No. 134108.
(115) Hammes-Schiffer, S. Nuclear-electronic orbital methods: Foundations and prospects. *J. Chem. Phys.* **2021**, *155*, No. 030901.
(116) Mukamel, S. Multidimensional Femtosecond Correlation Spectroscopies of Electronic and Vibrational Excitations. *Annu. Rev. Phys. Chem.* **2000**, *51*, 691.
(117) Hack, J. H.; Dombrowski, J. P.; Ma, X.; Chen, Y.; Lewis, N. H. C.; Carpenter, W. B.; Li, C.; Voth, G. A.; Kung, H. H.; Tokmakoff, A. Structural Characterization of Protonated Water Clusters Confined in HZSM-5 Zeolites. *J. Am. Chem. Soc.* **2021**, *143*, 10203−10213.
(118) Ahn, S.; Hong, M.; Sundararajan, M.; Ess, D. H.; Baik, M.-H. Design and Optimization of Catalysts Based on Mechanistic Insights Derived from Quantum Chemical Reaction Modeling. *Chem. Rev.* **2019**, *119*, 6509−6560.
(119) Schumaker, M. F.; Pomes, R.; Roux, B. A Combined Molecular Dynamics and Diffusion Model of Single Proton Conduction Through Gramicidin. *Biophys. J.* **2000**, *79*, 2840.
(120) Schumaker, M. F.; Pomes, R.; Roux, B. Framework Model for Single Proton Conduction Through Gramicidin. *Biophys. J.* **2001**, *80*, 12.
(121) Iyengar, S. S.; Petersen, M. K.; Day, T. J. F.; Burnham, C. J.; Teige, V. E.; Voth, G. A. The Properties of Ion-Water Clusters. I. the Protonated 21-Water Cluster. *J. Chem. Phys.* **2005**, *123*, No. 084309.

https://doi.org/10.1021/acs.jctc.3c00404
J. Chem. Theory Comput. 2023, 19, 6082−6092